Title

Slow-Injection Growth of Seeded CdSe/CdS Nanorods with Unity Fluorescence Quantum Yield and Complete Shell to Core Energy Transfer.

Journal

ACS nano, 10(3)

ISSN

1936-0851

Authors

Coropceanu, Igor
Rossinelli, Aurelio
Caram, Justin R
et al.

Publication Date

2016-03-01

DOI

10.1021/acsnano.5b06772

Peer reviewed

ACSNANO
www.acsnano.org
ARTICLE

Slow-Injection Growth of Seeded CdSe/CdS Nanorods with Unity Fluorescence Quantum Yield and Complete Shell to Core Energy Transfer

Igor Coropceanu,[†] Aurelio Rossinelli,[‡] Justin R. Caram,[†] Francesca S. Freyria,[†] and Moungi G. Bawendi*[,†]

[†]Department of Chemistry, Massachusetts Institute of Technology, Cambridge, Massachusetts 02139, United States
[‡]Optical Materials Engineering Laboratory, ETH Zurich, 8092 Zurich, Switzerland

Supporting Information

ABSTRACT: **A two-step process has been developed for growing the shell of CdSe/CdS core/shell nanorods. The method combines an established fast-injection-based step to create the initial elongated shell with a second slow-injection growth that allows for a systematic variation of the shell thickness while maintaining a high degree of monodispersity at the batch level and enhancing the uniformity at the single-nanorod level. The second growth step resulted in nanorods exhibiting a fluorescence quantum yield up to 100% as well as effectively complete energy transfer from the shell to the core. This improvement suggests that the second step is associated with a strong suppression of the nonradiative channels operating both before and after the thermalization of the exciton. This hypothesis is supported by the suppression of a defect band, ubiquitous to CdSe-based nanocrystals after the second growth.**

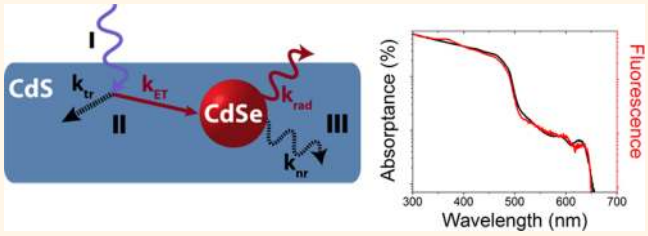

KEYWORDS: *CdSe/CdS, nanorod, optical downshifting*

The versatility of inorganic nanocrystals is greatly expanded by the possibility of modifying their electronic properties by changing not only their size, but also their dimensionality. In particular, elongated structures such as nanorods exhibit an attractive set of emergent properties that set them apart from spherical quantum dots, such as a large degree of fluorescence anisotropy[1,2] and enhanced transport through various types of biological tissues.[3] Among visible-light-emitting materials, seeded CdSe/CdS nanorods (structures consisting of a spherical CdSe core surrounded by an elongated CdS shell) have emerged as a robust material system combining a high degree of monodispersity with bright and spectrally narrow photoluminescence. However, while rapid initial progress in the development of CdSe/CdS nanorods resulted in the achievement of fluorescence quantum yields of up to 75%,[1,4] further improvement of the quantum yield proved elusive using conventional fast-injection-based preparations. Moreover, as with CdSe/CdS quantum dots, the quantum yield was rapidly observed to decrease with increasing shell volume, an effect that was attributed to the long radiative lifetimes caused by delocalization of the electron into the shell.[1] This reduction in the efficiency has been a significant barrier to these materials for a variety of optical and optoelectronic applications, such as luminescent solar concentrators (LSCs) and light-emitting diodes (LEDs).[5−9]

In this work, we have employed a two-step process to synthesize the shell by first using a hot injection reaction to grow a thin CdS layer, followed by a slow second growth. The first step is needed to maintain kinetic control over the initial growth of the shell in order to obtain a monodisperse batch of nanorods with a well-defined elongated geometry, as previously reported.[10] The second slow growth in turn was motivated by our previous work on spherical CdSe/CdS quantum dots, where a slow high-temperature growth was seen to improve both the synthetic and optical quality of the nanoparticles. In our study we show that the second growth step not only improved the crystallinity of the nanorods but had a major impact on the optical properties, increasing the fluorescence quantum yield up to unity, highly suppressing residual defect emission, and allowing for complete energy transfer from the shell to the core. Our approach highlights the benefits of decoupling the growth of anisotropic heterostructures into two steps: (1) a fast step needed to direct the shape and size of the

Received: October 27, 2015
Accepted: February 8, 2016
Published: February 17, 2016

DOI: 10.1021/acsnano.5b06772
ACS Nano 2016, 10, 3295−3301

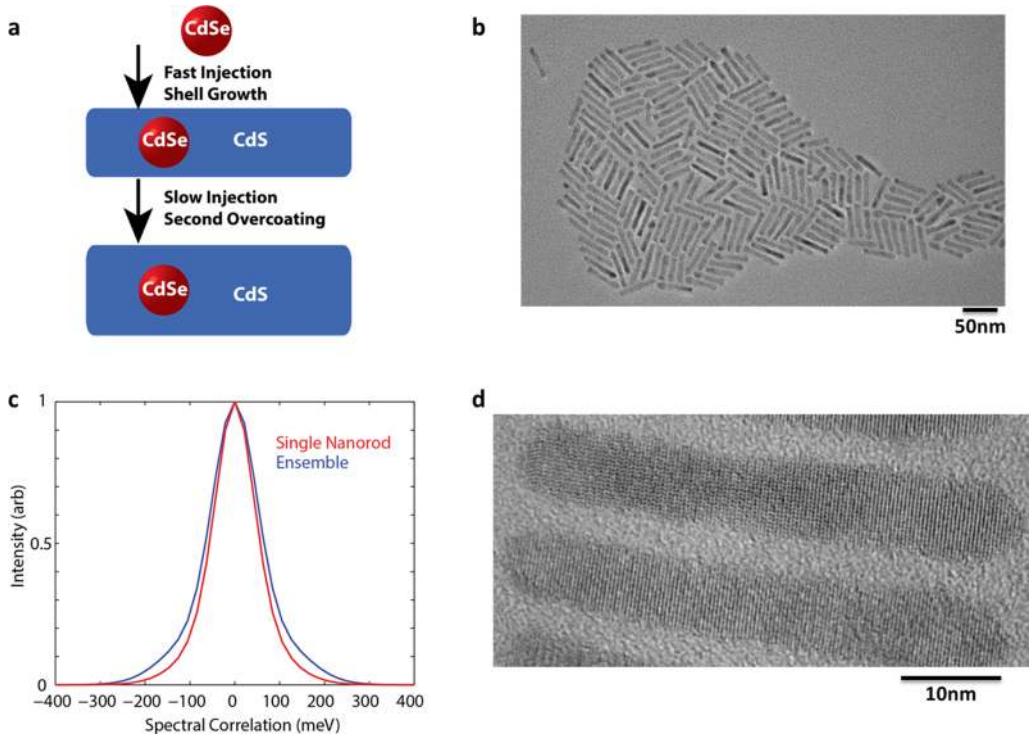

Figure 1. (a) General synthetic scheme for the synthesis of the seeded nanorods. (b) TEM micrograph after growth of the second shell (S1). (c) s-PCFS traces showing the ensemble and average single-nanorod spectral correlation of sample S1. (d) HRTEM of sample S2.

nanostructures and (2) a slow annealing step to reduce the defects introduced by the fast growth to highly suppress the nonradiative channels that reduce the fluorescence quantum yield.

RESULTS AND DISCUSSION

The general synthetic scheme for the shell growth is illustrated in Figure 1a. Spherical CdSe cores were first overcoated using an established fast-injection-based recipe[1] to yield thin-shelled CdSe/CdS nanorods with a high degree of monodispersity. These nanorods were then isolated, and in a second reaction the shell was grown further using a high-temperature, slow-injection reaction. The second growth provided two key advantages: (1) an increase in the fluorescence quantum yield and a suppression of the trap emission and (2) independent control of the shell thickness. This synthetic protocol resulted in nanorods that remained very monodisperse at the batch level even as the shell thickness was continuously increased. In order to study the effective monodisperisty of the sample as it relates to the optical properties of the system, the ensemble and average single-nanorod spectral correlations were measured using solution photon correlation Fourier spectroscopy (s-PCFS; see Figure 1c).[11] From the small difference between the two spectral correlations, one can readily conclude that the inhomogeneous broadening of the sample results in only a minor contribution to the overall spectral width. In addition, the particles were highly uniform and crystalline at the individual nanorod level, as can be seen from the high-resolution TEM in Figure 1d. The uniformity achieved after the second growth step appears to be a significant improvement from the initial nanorods, where the fast injection frequently results in the appearance of visible kinks as well as other crystallographic defects such as edge dislocations (see Figure S3).

In order to systematically study the evolution of the electronic and optical properties of the new nanorods, a size series was prepared by first creating a batch of nanorods using the conventional fast-injection-based growth (denoted F1),[1] which was then subjected to an additional slow growth step to create two new samples, which we denoted in the order of increasing thickness as S1 and S2. Finally in order to even more drastically increase the shell thickness, sample S1 was subjected to one additional slow growth, yielding the sample denoted S3. As can be seen from Table 1, the length of all four samples is almost unchanged (ranging from 40 to 45 nm), as additional growth along the axial direction was balanced by the general tendency of the particles to become more spherical after prolonged reaction times. In contrast, the thickness increased continuously from 5.5 nm for F1 to 6.3, 7.0, and 9.5 nm in S1, S2, and S3, respectively. By taking into account the initial size of the core (d = 4.9 nm) and the thickness of each individual CdS layer, we can estimate the change in the number of CdS monolayers (estimated assuming each layer of CdS had a thickness of 0.35 nm) to be from 1 in F1 to 2, 3, and 7 respectively in S1, S2, and S3.

Table 1. Dimensions and Fluorescence Quantum Efficiency of Nanorod Samples

sample	length (nm)	width (nm)	fluorescence lifetime (ns)	quantum yield (%)
F1	44 ± 4	5.5 ± 0.2	14	59 ± 1
S1	45 ± 3	6.3 ± 0.2	23	95 ± 1
S2	42 ± 3	7.0 ± 0.2	29	98 ± 2
S3	40 ± 3	9.5 ± 0.2	61	85 ± 1

The fluorescence spectra of these samples are shown in Figure 2a. As the shell volume was increased, the spectra continuously red-shifted and the line shapes slightly broadened

DOI: 10.1021/acsnano.5b06772
ACS Nano 2016, 10, 3295−3301

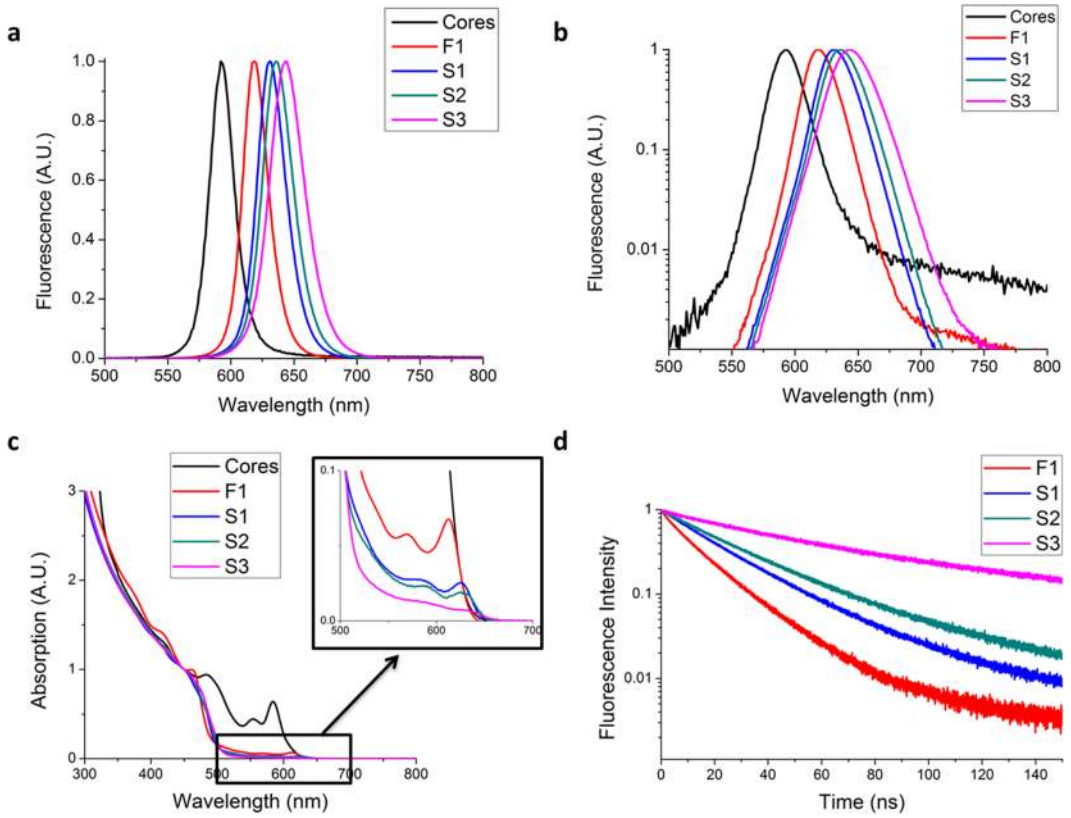

Figure 2. (a) Fluorescence spectra of the CdSe cores and the nanorods on a linear scale and (b) on a logarithmic scale. (c) Absorption spectra of nanorods (inset magnification of first excitonic feature.) (d) Time-resolved photoluminescence traces of the nanorod samples.

as expected from the known tendency of the electron to delocalize into the shell across the quasi-type-II barrier typical of CdSe/CdS heterostructures.[12,13] An interesting qualitative difference between the spectra is revealed when replotting the data on a logarithmic scale (Figure 2b). In addition to the band-edge luminescence, one can distinguish an additional red-shifted band in some of the spectra. Such a feature is ubiquitous to CdSe- or CdS-based nanoparticles, and while its origin has not been definitively identified, it is generally attributed to defect states either at the surface of the nanoparticle or at the core/shell interface and is for this reason usually denoted as the *trap band* in these materials.[14] What is interesting is that while this feature is strongly pronounced in the initial CdSe cores and still clearly apparent in the initial nanorods, this band is highly suppressed in the samples subjected to the second slow shell growth. Indeed the feature is essentially undetectable in the two thinner nanorod samples (S1 and S2) and only re-emerged in the thickest sample (S3), but even then remained much weaker than in the initial nanorods.

The observed reduction in the defect band can be linked to the large degree of uniformity and crystallinity of the shell and the improved passivation of the surface made possible by the slow growth step. Such a behavior is fully consistent with the improved optical performance obtained in our previous work on spherical CdSe/CdS quantum dots.[5,15] Importantly in the case of both the nanorods and the quantum dots the suppression of the defect band is not simply a function of the CdS shell thicknesss but always requires the slow growth step. This behavior can be clearly seen in the case of the CdSe/CdS QDs, where the fluorescence spectra for a series of aliquots are shown in Figure S7a/b, all grown using a high-temperature slow-injection growth as described in ref 5. No defect band is apparent in any of the spectra, even for the lowest shell thickness. In addition, samples of CdSe/CdS nanorods grown using the fast-injection growth from a smaller initial core do exhibit such a defect band (Figure S7c/d), even if the shell is thicker than when starting from a larger core as in our present study.[2] These observations highlight the fact that it is the use of a slow high-temperature growth step that is the key factor enabling the suppression of the defect band and the more general improvement in the optical properties.

The fluorescence quantum yield of the four nanorod samples were then measured using an integrating sphere (see Table 1). The excitation wavelength was selected to be 405 nm in order to ensure that the majority of the absorption occurred directly into the shell. The initial quantum yield of the nanorods after the first growth was only moderate, at 59%, which already represented a reduction from the higher values (70%+) measured for nanorods made from the same batch of cores but having a shorter shell. Upon growing a thin shell using the slow growth method (sample S1), the quantum yield increased to 95%. A similar sample having a thicker shell (S2) was measured to have a quantum yield of 98%. This significant increase in the quantum yield even as the shell volume was increased suggests a strong suppression of the nonradiative decay channels present in the initial nanorods. It was only when growing the shell further that the quantum yield decreased, a value of 85% being measured for the thickest-shelled nanorods in this series. This final decrease in the quantum yield may largely be due to the gradual lengthening of the radiative lifetime as the shell volume was increased (see Figure 2d),

DOI: 10.1021/acsnano.5b06772
ACS Nano 2016, 10, 3295−3301

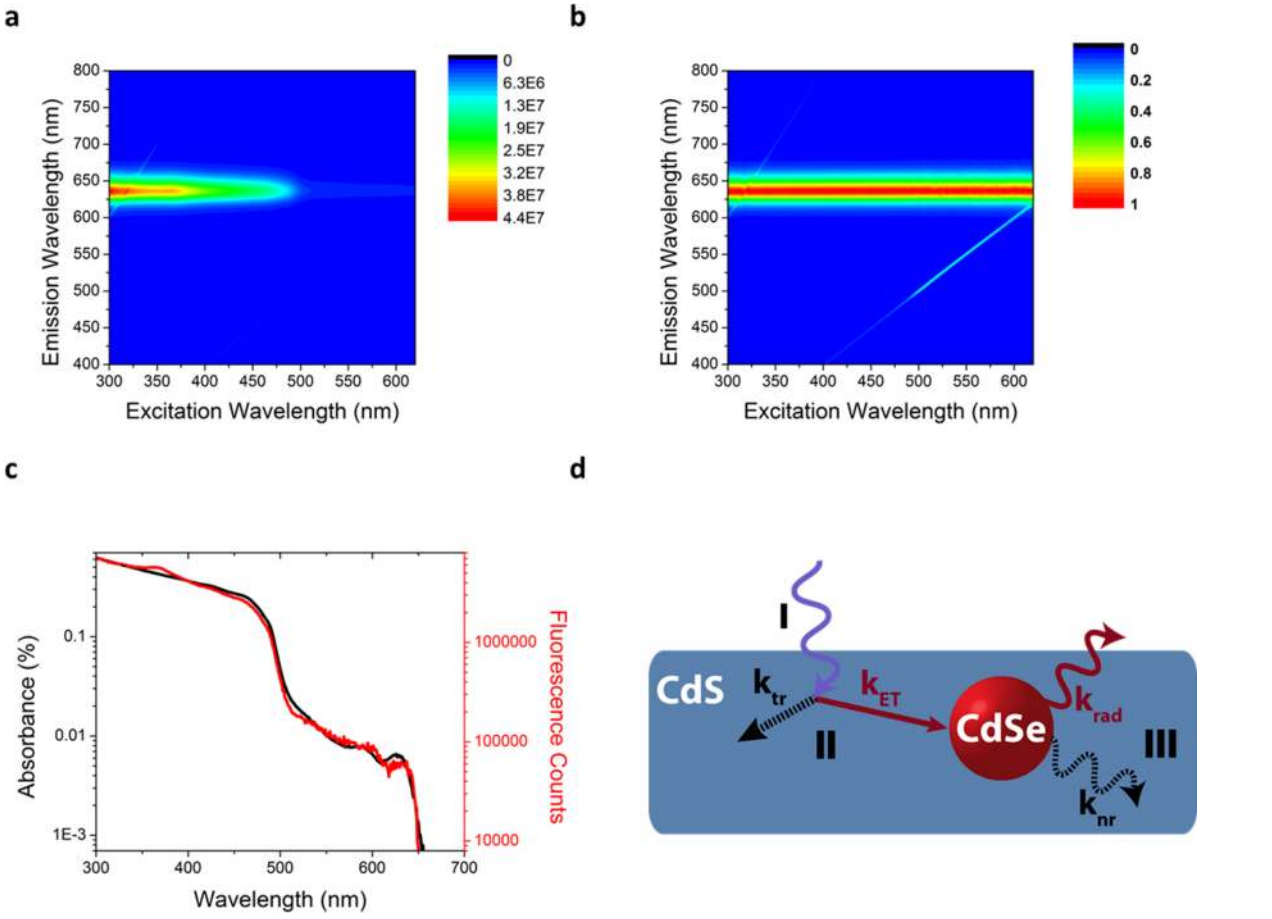

Figure 3. (a) Excitation−emission spectrum of CdSe/CdS nanorods (S2). (b) Normalized excitation−emission spectrum of S2. (c) Excitation spectrum and absorbance of S2. (d) Optoelectronic processes in CdSe/CdS nanorods.

which again made the remaining nonradiative decay channels competitive with radiative recombination.

The evolution of the normalized absorption spectra from the CdSe cores to the nanorod series is shown in Figure 2c. At high energies (above 500 nm), where most of the absorption is mediated by the CdS shell, the spectra remain relatively constant, barring the gradual disappearance of the sharp features as the CdS shell gradually transitions from the quasi-one-dimensional confinement to its bulk-like limit. However, as in the case of spherical CdSe/CdS quantum dots, the biggest change observed in the spectra consists in the relative reduction of the first excitonic features (see the inset of Figure 2c) compared to the CdS band as the volume of the shell increases and consequently the volumetric ratio of CdSe to CdS decreases.[5] Because virtually all of the spectral overlap between the emission and absorption spectra of the nanorods occurs through this first excitonic feature, its relative reduction directly leads to a decrease in the effective reabsorption of these materials. Indeed, for the sample with the largest shell volume (S3), the absorption at the fluorescence maximum is reduced by 2 orders of magnitude compared to its value in the CdS band. Such a low reabsorption is comparable to values previously reported for giant-shelled CdSe/CdS quantum dots and represents one of the lowest levels of reabsorption measured in inorganic or organic materials.

One additional advantage of dividing the shell growth into two steps is to allow for an independent control of the length and thickness of the nanorods, allowing for the synthesis of uniform particles with a wide range of aspect ratios for any particular length. While conventional fast growth techniques yield highly uniform particles with a tunable length, changing the thickness has proven to be much more challenging since varying most synthetic parameters such as the amount of precursors injected and the reaction time predominantly affects the length while leaving the thickness largely unchanged.[1,2] While some progress has been reported for preparing thicker shelled nanorods by using a higher injection temperature, this approach nevertheless still resulted in coupled growth of the nanorods along both their long and short axes.[16] In contrast, using our method, the first step results predominantly in growth along the long axis, while the second step occurs under conditions that promote symmetric growth in all directions.[10,15] Therefore, by carefully selecting the reaction conditions our method allows for core/shell nanorods with a desired combination of length and thickness. As a final note, because the shell is in equilibrium with the reaction precursors, under conditions that promote isotropic growth, particles tend to become rounder. As a result, during the second step, the length may remain constant or even decrease even as the volume is increasing. This fact should be taken into account when designing the growth of the shell in order to obtain the target dimensions.

One key property exhibited by the nanorods grown using the current method is that in contrast to other large-volume CdSe/CdS particles, they exhibit effectively complete energy transfer from the shell to the core. Such a result could be anticipated

DOI: 10.1021/acsnano.5b06772
ACS Nano 2016, 10, 3295−3301

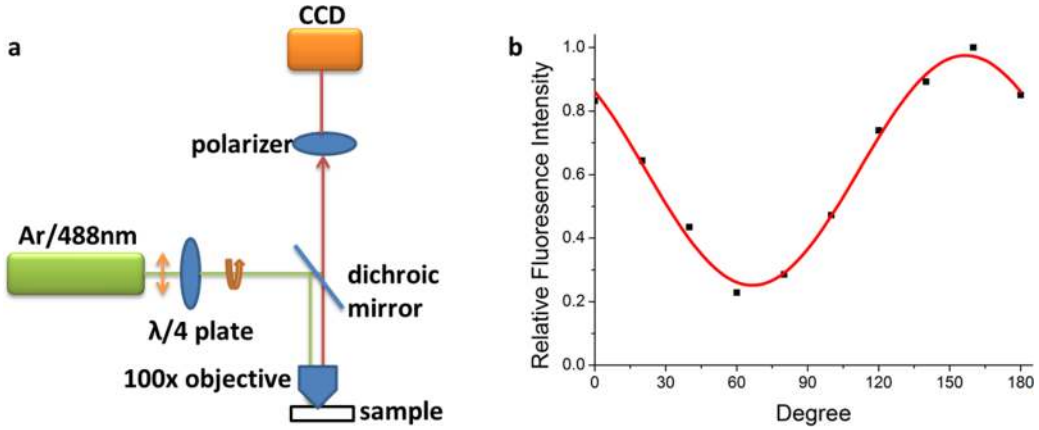

Figure 4. (a) Schematic of the setup used for polarization-dependent single-nanorod fluorescence spectroscopy. (b) Fluorescence intensity of sample T1 as a function of the polarizer angle.

from the fact that a unity quantum yield was measured even when exciting at 405 nm, where most of the absorption occurred directly into the shell. A more systematic demonstration of this property follows from the analysis of the excitation−emission spectrum of the nanorods, shown in Figure 3a, which shows the variation of the fluorescence spectrum of the nanorods as a function of the excitation wavelength. Upon normalizing the spectrum to the peak of the fluorescence at each excitation wavelength (Figure 3b), it is apparent that the spectrum remains completely unchanged, suggesting that the exciton is always able to equilibrate on a time scale much faster than the fluorescence lifetime. Upon taking a cross-section of the 2D plot prior to normalization (or equivalently directly measuring an excitation spectrum), the resulting spectrum tracks the absorbance spectrum completely. This property means that the quantum yield of the particles is insensitive to the excitation wavelength.

The fact that the energy transfer in these nanorods is significantly more efficient than in conventional nanorods of similar dimensions indicates that the slow growth step results in a suppression of the surface traps that can otherwise prevent the exciton from localizing to the core.[17] This general behavior can be understood within the general scheme shown in Figure 3d. If the nanorod is excited well above its effective band gap, the exciton that will be generated will mostly be delocalized in the CdS shell (I). In order for the exciton to eventually recombine radiatively in the core, it must successfully pass through two branching ratios. First, the hot exciton must localize in and around the core (II) upon thermalization (at an effective rate k_{ET}) in competition with the parasitic pathways that can trap the exciton or one of the charge carriers in the shell (at a rate k_{tr}). Finally, the exciton must recombine radiatively (III) at a rate k_{rad} in competition with all the remaining nonradiative decay channels (k_{nr}). Because both the localization rate[18] and the radiative rate are known to decrease with the shell volume, the fact that nanorods subjected to the slow growth step can exhibit a unity quantum yield when excited into the shell indicates a strong suppression of all the nonradiative channels operating both before and after the thermalization of the exciton. It should be pointed out that upon magnifying the spectral range around 500 nm, one can observe a very small peak as shown in Figure S8, presumably due to emission of light from the CdS shell prior to thermalization. The integrated area of this feature is about 10 000 times weaker than the integrated band-edge spectrum, which is consistent with the fact that the typical carrier localization time scale (∼40 ps) is about 1000−10 000 times shorter than the typical intrinsic radiative lifetime of CdS nanostructures (∼10 ns).

Finally, in order to assess the degree of polarization of the nanorods, we performed polarization-dependent single-particle fluorescence spectroscopy. In particular we were interested to see whether the thickest shell nanorods would exhibit the same degree of polarization (P, defined as the difference of the orthogonally polarized components of the fluorescence divided by the total fluorescence intensity) as the conventional, thinner nanorods obtained after the initial first injection. The experimental setup that was used is shown schematically in Figure 4a. The sample consisted of a dilute solution of nanorods spun cast onto a coverslip, which allowed for a clear separation between individual particles. The nanorods (sample T1, which was synthesized using a similar procedure to that used for sample S3) had a length of 63 nm and a thickness of 10 nm, resulting in an aspect ratio (the ratio of the length to the width) of approximately 6. A typical trace showing variation of the fluorescence intensity as a function of the polarizer angle is shown in Figure 4b, from which the degree of polarization can be estimated to be ∼65%. This value is comparable to values that have been previously reported for nanorods that had a similar aspect ratio, but with a thinner shell (and a proportionately shorter length). Such a result is consistent with the theoretically predicted component of the fluorescence polarization that is attributable to the dielectric environment, as this contribution should depend only on the aspect ratio rather on the ratio of the length and the width of the shell, rather on their absolute dimensions.[19]

CONCLUSION

In conclusion, we have developed a two-step method to grow an elongated CdS shell on CdSe cores, yielding highly monodisperse nanorods with tunable shell thickness and near-unity quantum yields. The nanorods also exhibited highly efficient energy transfer from the shell to the core, making the structures well-suited for broadband light harvesting. The improvement in the optical properties of the system may be attributed to the increased uniformity and crystallinity of the shell made possible by the long reaction time of the second growth. This result extends the same optimization that we previously reported for spherical giant-shelled CdSe/CdS particles to a quasi-one-dimensional geometry where the

DOI: 10.1021/acsnano.5b06772
ACS Nano 2016, 10, 3295−3301

good optical properties can be combined with linear polarization. We believe that these new materials may be good candidates for a variety of optical applications such as luminescent downshifting and luminescent solar concentrators.[5,20]

MATERIALS AND METHODS

Synthesis. The synthesis of the CdSe cores and the first fast-injection shell growth were carried out by following a previously published synthetic recipe. The second step of the shell growth consisted of a slow high-temperature CdS growth, adapted from ref 5 and is described in detail in the Supporting Information.

Optical Imaging. Absorption spectra were recorded using a Cary 5000 spectrophotometer, and emission spectra were recorded using a Fluoromax-3 spectrofluorometer. Quantum yield measurements were taken using a Labsphere integrating sphere using a 5 mW, 405 nm light as the source, chopping the beam at 210 Hz, and collecting the output using a calibrated silicon detector through a Stanford Research Systems lock-in amplifying system. A filter was used to spectrally separate the fluorescence, and the final quantum yield was corrected for reflectance and leakage of the filter.

Time-Resolved Photoluminescence. To measure the PL lifetime, the nanorods were diluted in a hexane solution, placed in a quartz cuvette, and excited with a pulsed 532 nm laser (PicoQuant) at a 2.5 MHz repetition rate. The excitation light was removed using a spectral filter, and the emission was collected by a single-photon avalanche photodiode (Micro Photon Devices). The photon arrival time was correlated with the excitation pulse by a Picoharp 300 (PicoQuant) time-correlated single-photon-counting system.

Single-Particle Fluorescence. The excitation source was a beam of 488 nm light from an argon ion laser, which was rendered circularly polarized using a quarter-wave plate and then focused onto the sample using a 100× oil immersion objective. The emitted light was passed through a polarizer and was finally collected by a CCD camera. The fluorescence was connected with 30 s integration windows for each data point as the polarizer was moved stepwise by 20° from 0° to 0°.

ASSOCIATED CONTENT

Supporting Information

The Supporting Information is available free of charge on the ACS Publications website at DOI: 10.1021/acsnano.5b06772.

Synthetic details, a description of the polarization-dependent single-nanorod spectroscopy, TEM micrographs of the CdSe cores and the CdSe/CdS nanorods, fluorescence spectra of aliquots of a CdSe/CdS QD growth, and the fluorescence spectrum of a CdSe/CdS nanorod sample with a small CdSe core (PDF)

AUTHOR INFORMATION

Corresponding Author

*E-mail: mgb@mit.edu.

Notes

The authors declare no competing financial interest.

ACKNOWLEDGMENTS

I.C. gratefully acknowledges support from the National Science Foundation Graduate Fellowship. The work has been supported by Eni SpA under the Eni-MIT Alliance Solar Frontiers Center. J.R.C. is funded in part by the DOE Office of Science, Basic Energy Sciences, under Award No. DE-FG02-07ER46454. The authors would like to thank Whitney Hess and Chia-Hao Chuang for valuable discussions regarding the manuscript and Mark Wilson for help in taking part of the time-resolved PL data. Part of this work made use of the MRSEC Shared Experimental Facilities at the MIT Center for Materials Science and Engineering (CMSE), supported by the National Science Foundation under award number DMR-08-19762.

REFERENCES

(1) Carbone, L.; Nobile, C.; De Giorgi, M.; Sala, F. D.; Morello, G.; Pompa, P.; Hytch, M.; Snoeck, E.; Fiore, A.; Franchini, I. R.; Nadasan, M.; Silvestre, A. F.; Chiodo, L.; Kudera, S.; Cingolani, R.; Krahne, R.; Manna, L. Synthesis and Micrometer-Scale Assembly of Colloidal Cdse/Cds Nanorods Prepared by a Seeded Growth Approach. *Nano Lett.* **2007**, *7*, 2942−2950.

(2) Talapin, D. V.; Koeppe, R.; Gotzinger, S.; Kornowski, A.; Lupton, J. M.; Rogach, A. L.; Benson, O.; Feldmann, J.; Weller, H. Highly Emissive Colloidal Cdse/Cds Heterostructures of Mixed Dimensionality. *Nano Lett.* **2003**, *3*, 1677−1681.

(3) Chauhan, V. P.; Popović, Z.; Chen, O.; Cui, J.; Fukumura, D.; Bawendi, M. G.; Jain, R. K. Fluorescent Nanorods and Nanospheres for Real-Time in Vivo Probing of Nanoparticle Shape-Dependent Tumor Penetration. *Angew. Chem., Int. Ed.* **2011**, *50*, 11417−11420.

(4) Sitt, A.; Hadar, I.; Banin, U. Band-Gap Engineering, Optoelectronic Properties and Applications of Colloidal Heterostructured Semiconductor Nanorods. *Nano Today* **2013**, *8*, 494−513.

(5) Coropceanu, I.; Bawendi, M. G. Core/Shell Quantum Dot Based Luminescent Solar Concentrators with Reduced Reabsorption and Enhanced Efficiency. *Nano Lett.* **2014**, *14*, 4097−4101.

(6) Bronstein, N. D.; Li, L.; Xu, L.; Yao, Y.; Ferry, V. E.; Alivisatos, A. P.; Nuzzo, R. G. Luminescent Solar Concentration with Semiconductor Nanorods and Transfer-Printed Micro-Silicon Solar Cells. *ACS Nano* **2014**, *8*, 44−53.

(7) Bradshaw, L. R.; Knowles, K. E.; McDowall, S.; Gamelin, D. R. Nanocrystals for Luminescent Solar Concentrators. *Nano Lett.* **2015**, *15*, 1315−1323.

(8) Castelli, A.; Meinardi, F.; Pasini, M.; Galeotti, F.; Pinchetti, V.; Lorenzon, M.; Manna, L.; Moreels, I.; Giovanella, U.; Brovelli, S. High-Efficiency All-Solution-Processed Light-Emitting Diodes Based on Anisotropic Colloidal Heterostructures with Polar Polymer Injecting Layers. *Nano Lett.* **2015**, *15*, 5455−5464.

(9) Di Stasio, F.; Grim, J. Q.; Lesnyak, V.; Rastogi, P.; Manna, L.; Moreels, I.; Krahne, R. Single-Mode Lasing from Colloidal Water-Soluble Cdse/Cds Quantum Dot-in-Rods. *Small* **2015**, *11*, 1328−1334.

(10) Carbone, L.; Cozzoli, P. D. Colloidal Heterostructured Nanocrystals: Synthesis and Growth Mechanisms. *Nano Today* **2010**, *5*, 449−493.

(11) Cui, J.; Beyler, A. P.; Marshall, L. F.; Chen, O.; Harris, D. K.; Wanger, D. D.; Brokmann, X.; Bawendi, M. G. Direct Probe of Spectral Inhomogeneity Reveals Synthetic Tunability of Single-Nanocrystal Spectral Linewidths. *Nat. Chem.* **2013**, *5*, 602−606.

(12) Brovelli, S.; Schaller, R. D.; Crooker, S. A.; García-Santamaría, F.; Chen, Y.; Viswanatha, R.; Hollingsworth, J. A.; Htoon, H.; Klimov, V. I. Nano-Engineered Electron−Hole Exchange Interaction Controls Exciton Dynamics in Core−Shell Semiconductor Nanocrystals. *Nat. Commun.* **2011**, *2*, 280.

(13) Christodoulou, S.; Vaccaro, G.; Pinchetti, V.; De Donato, F.; Grim, J. Q.; Casu, A.; Genovese, A.; Vicidomini, G.; Diaspro, A.; Brovelli, S.; Manna, L.; Moreels, I. Synthesis of Highly Luminescent Wurtzite Cdse/Cds Giant-Shell Nanocrystals Using a Fast Continuous Injection Route. *J. Mater. Chem. C* **2014**, *2*, 3439−3447.

(14) Kambhampati, P. On the Kinetics and Thermodynamics of Excitons at the Surface of Semiconductor Nanocrystals: Are There Surface Excitons? *Chem. Phys.* **2015**, *446*, 92−107.

(15) Chen, O.; Zhao, J.; Chauhan, V. P.; Cui, J.; Wong, C.; Harris, D. K.; Wei, H.; Han, H. S.; Fukumura, D.; Jain, R. K.; Bawendi, M. G. Compact High-Quality Cdse-Cds Core-Shell Nanocrystals with Narrow Emission Linewidths and Suppressed Blinking. *Nat. Mater.* **2013**, *12*, 445−451.

(16) Pisanello, F.; Leménager, G.; Martiradonna, L.; Carbone, L.; Vezzoli, S.; Desfonds, P.; Cozzoli, P. D.; Hermier, J.-P.; Giacobino, E.; Cingolani, R.; De Vittorio, M.; Bramati, A. Non-Blinking Single-Photon Generation with Anisotropic Colloidal Nanocrystals: Towards

DOI: 10.1021/acsnano.5b06772
ACS Nano 2016, 10, 3295−3301

Room-Temperature, Efficient, Colloidal Quantum Sources. *Adv. Mater.* **2013**, *25*, 1974−1980.
(17) Wu, K.; Hill, L. J.; Chen, J.; McBride, J. R.; Pavlopolous, N. G.; Richey, N. E.; Pyun, J.; Lian, T. Universal Length Dependence of Rod-to-Seed Exciton Localization Efficiency in Type I and Quasi-Type II Cdse@Cds Nanorods. *ACS Nano* **2015**, *9*, 4591−4599.
(18) She, C.; Demortière, A.; Shevchenko, E. V.; Pelton, M. Using Shape to Control Photoluminescence from Cdse/Cds Core/Shell Nanorods. *J. Phys. Chem. Lett.* **2011**, *2*, 1469−1475.
(19) Shabaev, A.; Efros, A. L. 1d Exciton Spectroscopy of Semiconductor Nanorods. *Nano Lett.* **2004**, *4*, 1821−1825.
(20) Meinardi, F.; Colombo, A.; Velizhanin, K. A.; Simonutti, R.; Lorenzon, M.; Beverina, L.; Viswanatha, R.; Klimov, V. I.; Brovelli, S. Large-Area Luminescent Solar Concentrators Based on`Stokes-Shift-Engineered' Nanocrystals in a Mass-Polymerized Pmma Matrix. *Nat. Photonics* **2014**, *8*, 392−399.

DOI: 10.1021/acsnano.5b06772
ACS Nano 2016, 10, 3295−3301